ISSN: 2476-6909; Modares. Mech. Eng. 2027;27(04):283-295.

Modares Mechanical Engineering

DOI: 10.48311/mme.2026.121701.83050
journal homepage: mme.modares.ac.ir

Investigation of the Effect of Loading Rate on the Tensile Behavior of GFRP-Strengthened Steel Pipes under Stepwise Loading

Ramin Beyranvand, Mehdi Ansari*

Mechanical Engineering Department, Arak University of Technology, Arak, Iran

ARTICLE INFO

Article Type
Original Research

Article History
Received: June 30, 2026
Revised: August 09, 2026
Accepted: August 11, 2026
ePublished: November 11, 2026

ABSTRACT

Under actual service conditions, particularly during natural hazards, loads acting on pipelines are often applied rapidly, intermittently, and in successive stages rather than in a uniform and standardized manner. In this study, to simulate this realistic loading pattern, the mechanical behavior of GFRP-strengthened steel pipes subjected to stepwise tensile loading with intermediate holding periods was investigated at loading rates of 50, 100, 150, and 200 mm/min. The primary objective was to evaluate the effects of loading rate and stepwise loading history on the ultimate joint capacity. The results showed that the maximum shear stresses under stepwise loading at loading rates of 50, 100, 150, and 200 mm/min were 5.485, 4.463, 4.724, and 4.424 MPa, respectively. Although the overall trend of the results indicates a reduction in ultimate capacity with increasing loading rate, a slight increase in shear stress was observed at 150 mm/min compared with that at 100 mm/min. Comparison of the different loading stages also showed that the initial stages were the most sensitive to increasing loading rate; in Stage 1, the shear stress at loading rates of 100, 150, and 200 mm/min was 55%, 66%, and 82% lower, respectively, than that at 50 mm/min. Analysis of stress relaxation further showed that the magnitude of stress reduction during the holding periods decreased with increasing loading rate; in Stage 1, the stress reduction at 100, 150, and 200 mm/min was 24%, 55%, and 70% lower, respectively, than that at 50 mm/min. Overall, the results indicate that increasing the loading rate generally leads to a reduction in load-carrying capacity and a decrease in stress reduction during the holding periods, with these effects being more pronounced during the early stages of stepwise loading than during the later stages.

Keywords: GFRP, Bending, Stepwise Loading, Shear Stress, Stress Relaxation, Loading Rate

How to cite this article
Beyranvand R, Ansari M, Investigation of the Effect of Loading Rate on the Tensile Behavior of GFRP-Strengthened Steel Pipes under Stepwise Loading. Modares Mechanical Engineering; 2027;27(04):283-295.

*Corresponding author's email: ansari@arakut.ac.ir
*Corresponding ORCID ID: 0000-0002-8518-8609

Copyright© 2027, TMU Press. This open-access article is published under the terms of the Creative Commons Attribution-NonCommercial 4.0 International License which permits Share (copy and redistribute the material in any medium or format) and Adapt (remix, transform, and build upon the material) under the Attribution-NonCommercial terms.

شاپا: ۶۹۰۹-۲۴۷۶؛ مهندسی مکانیک مدرس. ۲۹۵-۲۸۳:(۰۴)۲۷؛۱۴۰۶

مهندسی مکانیک مدرس

DOI: 10.48311/mme.2026.121701.83050

صفحه اصلی مجله: mme.modares.ac.ir

بررسی اثر نرخ بارگذاری بر رفتار کششی لوله‌های فولادی تقویت‌شده با GFRP تحت بارگذاری مرحله‌ای

رامین بیرانوند، مهدی انصاری*

دانشکده مهندسی مکانیک، گروه ساخت و تولید، دانشگاه صنعتی اراک، اراک، ایران

اطلاعات مقاله

نوع مقاله
مقاله پژوهشی

تاریخچه مقاله
دریافت: ۱۴۰۵/۰۴/۰۹
بازنگری: ۱۴۰۵/۰۵/۱۸
پذیرش: ۱۴۰۵/۰۵/۲۰
ارائه آنلاین: ۱۴۰۵/۰۸/۲۰

چکیده

در شرایط واقعی بهره‌برداری و به‌ویژه در حوادث طبیعی، بارگذاری وارد بر خطوط لوله غالباً به‌صورت سریع، ناپیوسته و در گام‌های زمانی متوالی اعمال می‌شود، نه به‌شکل یکنواخت و استاندارد آزمایشگاهی. در این پژوهش، به‌منظور شبیه‌سازی این الگوی بارگذاری واقعی، رفتار مکانیکی لوله‌های فولادی تقویت‌شده با GFRP تحت بارگذاری کششی مرحله‌ای همراه با توقف‌های زمانی در نرخ‌های ۵۰، ۱۰۰، ۱۵۰ و ۲۰۰ میلی‌متر بر دقیقه بررسی شد. هدف اصلی، ارزیابی تأثیر نرخ بارگذاری و تاریخچه بارگذاری مرحله‌ای بر ظرفیت نهایی اتصال بود. نتایج نشان داد که بیشینه تنش برشی در بارگذاری مرحله‌ای برای نرخ‌های ۵۰، ۱۰۰، ۱۵۰ و ۲۰۰ میلی‌متر بر دقیقه به‌ترتیب برابر با ۵/۴۸۵، ۴/۴۶۳، ۴/۷۲۴ و ۴/۴۲۴ مگاپاسکال است. اگرچه روند کلی نتایج نشان‌دهنده کاهش ظرفیت نهایی با افزایش نرخ بارگذاری است، در نرخ ۱۵۰ میلی‌متر بر دقیقه افزایش جزئی تنش برشی نسبت به نرخ ۱۰۰ میلی‌متر بر دقیقه مشاهده شد. همچنین مقایسه مراحل مختلف بارگذاری نشان داد که مراحل ابتدایی بیشترین حساسیت را به افزایش نرخ دارند؛ به‌طوری‌که در مرحله اول، تنش در نرخ‌های ۱۰۰، ۱۵۰ و ۲۰۰ میلی‌متر بر دقیقه به‌ترتیب ۵۵، ۶۶ و ۸۲ درصد کمتر از نرخ ۵۰ بود. بررسی استراحت تنش نیز نشان داد که با افزایش نرخ بارگذاری، میزان افت تنش در دوره‌های توقف کاهش می‌یابد؛ به‌گونه‌ای که در مرحله اول، افت تنش در نرخ‌های ۱۰۰، ۱۵۰ و ۲۰۰ به‌ترتیب ۲۴، ۵۵ و ۷۰ درصد کمتر از نرخ ۵۰ اندازه‌گیری شد. بر اساس نتایج این پژوهش، افزایش نرخ بارگذاری در مجموع موجب کاهش ظرفیت تحمل تنش و کاهش میزان افت تنش در دوره‌های توقف شده و اثر آن در مراحل ابتدایی بارگذاری مرحله‌ای، محسوس‌تر از مراحل پایانی است.

کلیدواژه‌ها: GFRP، بارگذاری مرحله‌ای، تنش برشی، استراحت تنش، نرخ بارگذاری

نحوه ارجاع به این مقاله

بیرانوند رامین، انصاری مهدی، بررسی اثر نرخ بارگذاری بر رفتار کششی لوله‌های فولادی تقویت‌شده با GFRP تحت بارگذاری مرحله‌ای، مهندسی مکانیک مدرس. ۲۹۵-۲۸۳:(۰۴)۲۷؛۱۴۰۶.

*پست الکترونیکی نویسنده عهده‌دار مکاتبات: ansari@arakut.ac.ir

*شناسه ارکید نویسنده عهده‌دار مکاتبات: 0000-0002-8518-8609

Copyright© 2027, TMU Press. This open-access article is published under the terms of the Creative Commons Attribution-NonCommercial 4.0 International License which permits Share (copy and redistribute the material in any medium or format) and Adapt (remix, transform, and build upon the material) under the Attribution-NonCommercial terms.

1- Introduction

Pipelines are among the most critical infrastructures for fluid transportation due to their continuous operation, high transmission capacity, and economic efficiency. The operational stability and safety of these systems depend directly on the mechanical behavior of pipe sections, which serve as the primary load-bearing components in both onshore and offshore facilities [1, 2]. However, complex service conditions, internal pressure, cyclic loading, and various environmental factors can progressively degrade the structural performance and durability of these systems over time. In metallic pipelines, corrosion is recognized as one of the primary deterioration mechanisms, leading to a reduction in load-carrying capacity, an increased risk of leakage, and a shortened service life of the pipeline [3]. To mitigate this issue, various protection strategies, including protective coatings, cathodic protection, and chemical corrosion inhibitors, have been widely employed. Nevertheless, these approaches do not always provide adequate long-term protection, particularly under severe environmental conditions and prolonged service exposure [4]. Consequently, the use of composite materials has gained increasing attention in recent years as a complementary or alternative solution for enhancing the structural performance and extending the service life of pipelines. These materials have already been implemented in various oil and gas transmission systems and are considered promising candidates owing to their excellent resistance to corrosive environments [5]. Among composite materials, fiber-reinforced polymers (FRPs) have emerged as one of the most widely utilized material systems in engineering applications. Owing to their low density, high specific strength, excellent corrosion resistance, and the ability to tailor their mechanical properties, FRP composites have been extensively employed across a broad range of industrial applications [6, 7]. In addition to their technical advantages, the application of these materials is consistent with sustainable development strategies, as they can reduce maintenance costs and extend the service life of engineering systems. However, issues such as energy consumption during manufacturing and recycling challenges remain important considerations associated with their widespread use [8]. In recent years, FRP composites have been increasingly employed for the strengthening and rehabilitation of existing pipelines, as well as for the development of hybrid pipe systems, providing an effective approach to enhancing the structural reliability of pipeline infrastructures [9]. In this context, several experimental studies have also investigated the performance of metal–composite hybrid systems under quasi-static loading. One such study on glass fiber-reinforced aluminum/composite hybrid tubes showed that the overlap ratio of the composite layers can influence the energy-absorption capacity and crushing performance of the structure. These findings highlight the importance of the arrangement and interaction between metallic and composite components in determining the mechanical performance of hybrid systems [10]. Furthermore, experimental studies have shown that the mechanical performance of FRP-strengthened steel pipes can be affected by prior loading history and environmental exposure. Pre-damage and cyclic loading may alter the subsequent load-carrying capacity, while environmental conditions can further influence the mechanical response of the strengthened system. These findings highlight the importance of considering previous loading history and service conditions when evaluating the mechanical performance of FRP-strengthened pipelines [11]. In addition, numerous studies have demonstrated that FRP-based systems can significantly enhance the mechanical performance of structural components. For example, the incorporation of GFRP tubes in confined structural systems has been shown to improve the load-carrying capacity of the core material under dynamic loading conditions while mitigating the extent of structural damage [12]. Despite their significant advantages, the mechanical and structural behavior of FRP composites under various service conditions has remained the subject of extensive research. Several studies have investigated the performance of hybrid systems combining composite materials with other structural components, demonstrating that such systems can provide satisfactory load-carrying capacity and structural stability. Nevertheless, their behavior under specific conditions, such as elevated temperatures, still requires further investigation [13].

Furthermore, the application of FRP-based strengthening systems in various structural members has demonstrated that these materials, owing to their high tensile strength and excellent corrosion resistance, can significantly enhance the durability of engineering systems. Nevertheless, a comprehensive understanding of their mechanical properties and the development of appropriate methodologies for evaluating their structural behavior remain important research topics [14].

Meanwhile, several studies have reported that FRP-strengthened systems may exhibit failure mechanisms different from those of conventional structural systems when subjected to compressive loading and, in some cases, may possess lower ductility [15].

In addition to their mechanical characteristics, environmental conditions play a critical role in the long-term performance of composite materials. In humid or marine environments, the gradual ingress of moisture into the composite structure becomes more pronounced. Moisture absorption by the polymer matrix can progressively induce microstructural discontinuities, weaken the fiber–matrix interfacial bonding, and reduce the internal integrity of the composite, ultimately compromising the mechanical performance and long-term durability of FRP-strengthened systems [16, 17]. This issue becomes even more critical in systems continuously exposed to humid or corrosive environments. In addition to environmental effects, the time-dependent behavior of polymer composites represents another key factor governing their long-term structural performance. Although numerous studies have investigated the use of FRP composites for strengthening steel pipelines, most have primarily focused on their immediate or short-term mechanical response, while their long-term time-dependent behavior has received comparatively limited attention. Under actual service conditions, pipelines are frequently subjected to cyclic, intermittent, and stepwise loading, all of which may significantly influence their long-term performance. Owing to the viscoelastic nature of polymer matrices, time-dependent phenomena such as creep and stress relaxation are unavoidable. These mechanisms can alter the stress transfer process and the redistribution of internal forces at the steel–composite interface, leading to a gradual degradation of the load-carrying capacity of the strengthened system. Even thermosetting resins such as epoxy exhibit viscoelastic behavior, the extent of which depends on factors including the polymer network architecture and the degree of curing and may persist over extended periods. Therefore, a thorough understanding of these time-dependent mechanisms is essential for accurately predicting the long-term performance and durability of FRP-strengthened pipeline systems [18-20]. In the authors' previous study [21], the time-dependent behavior and stress relaxation of API 5L X42 seamless steel pipes strengthened with glass fiber-reinforced polymer (GFRP) composites were investigated under single-step and multi-step loading conditions. The primary focus of that study was to examine stress relaxation during the holding periods, the effects of loading rate and loading history on the time-dependent response, and the role of the viscoelastic behavior of the epoxy matrix in stress redistribution between the steel pipe and the composite layer. The results also showed that increasing the number of loading steps could alter the stress relaxation trend and promote the development of a quasi-stable mechanical state [21]. However, that study primarily addressed the time-dependent and stress relaxation aspects of the strengthened system, while the influence of loading rate on the evolution of shear stress throughout the loading stages and the ultimate load-carrying capacity of the system was not investigated in detail.

Accordingly, the present study extends the previous work [21] by focusing on the effect of loading rate on the tensile behavior and load-carrying capacity of GFRP-strengthened steel pipes subjected to stepwise loading. Tests were conducted at loading rates of 50, 100, 150, and 200 mm/min. In addition to evaluating stress reduction during the holding periods, the shear stress at the end of each loading stage, its evolution throughout the successive stages, and the maximum shear stress at failure were compared. Therefore, the main distinction between the present study and the previous work [21] lies in the emphasis on the relationship between loading rate, stage-by-stage tensile response, and ultimate load-carrying capacity, whereas the previous study primarily focused on the time-dependent behavior and stress relaxation of the system. This approach provides a more comprehensive understanding of the mechanical response of the GFRP–steel system under stepwise loading at different loading rates.
Accordingly, the objective of the present study is to experimentally evaluate the tensile behavior and load-carrying capacity of GFRP-strengthened steel pipes subjected to stepwise loading at different loading rates. To achieve this objective, stepwise tensile tests were performed at loading rates of 50, 100, 150, and 200 mm/min, with prescribed 10-min holding periods between successive loading stages. The effects of loading rate were evaluated by comparing the shear stress attained at the end of each loading stage, the stress reduction during the holding periods, and the ultimate shear stress at failure. The study also examines how the loading history and the accumulation of displacement through successive loading stages affect the mechanical response of the strengthened joint. The novelty of the present work lies in the systematic experimental assessment of the combined effects of loading rate and stepwise loading history on the tensile response, stage-by-stage shear stress evolution, stress relaxation, and ultimate load-carrying capacity of GFRP-strengthened steel pipes under a constant cumulative displacement of 3 mm. This approach provides a direct basis for comparing the mechanical response of the strengthened system at different loading rates and offers further insight into its behavior under intermittent and stepwise loading conditions relevant to practical service environments.

2- Materials and Fabrication Procedure

2-1- Materials

In this study, seamless API-5L X42 steel pipes were used as the substrate material for specimen fabrication. This steel grade was selected because of its adequate mechanical strength, uniform microstructure, and the absence of weld seams, thereby eliminating the influence of weld-induced discontinuities on the mechanical response of the strengthened specimens. To ensure effective bonding between the steel substrate and the composite overwrap, the outer surface of the pipes was carefully prepared prior to the strengthening process. First, the surface was uniformly abraded using sandpaper to remove surface contaminants and to increase the surface roughness required for improved mechanical adhesion. The prepared surfaces were subsequently cleaned with thinner, followed by acetone, to remove grease, dust, and any remaining contaminants. Finally, the specimens were allowed to dry at room temperature before the lay-up process to ensure complete evaporation of the cleaning solvents. An LR620 epoxy resin was employed as the polymer matrix of the composite system. This resin was selected because of its excellent adhesion to metallic substrates, good fiber impregnation capability, and suitability for the hand lay-up fabrication process. The reinforcing layer consisted of E-glass fiber mat with an areal density of 200 g/m² and a 7 × 8 woven architecture. This type of reinforcement provides a balanced distribution of fibers in the two principal directions, resulting in an appropriate combination of mechanical strength, formability, and ease of fabrication. Furthermore, the mat architecture facilitates more uniform resin impregnation during manufacturing, thereby improving the quality and structural integrity of the composite laminate.

2-2- Specimen Fabrication Procedure

The strengthened specimens were fabricated using seamless API-5L X42 steel pipes cut into sections of 150 mm in length. After cutting, both ends of each section were ground to remove cutting-induced irregularities and to obtain smooth and uniform surfaces at the joint interface. To ensure adequate adhesion between the steel substrate and the composite layer, the pipe surfaces were prepared prior to the strengthening process. The outer surfaces were uniformly abraded using sandpaper to remove oxide layers, possible corrosion products, and other surface contaminants while providing sufficient surface roughness to enhance mechanical interlocking. Subsequently, the prepared surfaces were cleaned and degreased with thinner, followed by acetone, to eliminate residual particles and contaminants, thereby ensuring suitable conditions for resin application.
Following surface preparation, two pipe sections were joined using an epoxy adhesive to form an integral specimen. The joint region was then strengthened with a glass fiber-reinforced polymer (GFRP) composite. For this purpose, LR620 epoxy resin and its hardener were mixed according to the manufacturer's recommended mixing ratio of 10:2 (by volume) to obtain a homogeneous mixture. A thin layer of resin was first applied to the prepared surface, after which E-glass fiber mat, fully impregnated with the epoxy resin, was wrapped around the joint region using the hand lay-up technique. The strengthened region extended 70 mm from the end of the first pipe section and 70 mm from the beginning of the second section, placing the bonded joint at the center of the composite wrap and resulting in a total reinforcement length of 140 mm.
To achieve consistent fabrication conditions across all specimens, 15 layers of glass fiber reinforcement were applied to each specimen. Based on the thickness of each individual layer and the total number of layers, the final thickness of the composite jacket after curing was approximately 3 mm. The hand lay-up process was performed with high precision and carefully controlled throughout the entire strengthening region, with particular attention paid to maintaining uniform layer thickness, adequate fiber impregnation with resin, and as uniform a composite distribution as possible along the strengthened region. All specimens were fabricated by the same operator using identical raw materials, a constant resin-to-hardener ratio, and the same fabrication procedure. During the lay-up process, the positioning and compaction of the individual layers were carefully controlled to minimize the formation of locally excessive thickness, resin-rich regions, or resin-deficient areas. After completion of the lay-up process, the final thickness of the composite jacket was also checked to ensure an appropriate degree of uniformity along the strengthened region. Despite these controls, minor and unavoidable variations in layer thickness and resin distribution may still occur due to the inherent nature of the hand lay-up technique. After completion of the lay-up process, the strengthened specimens were cured at room temperature for 24 h to allow the initial curing of the epoxy resin and stabilization of the mechanical properties of the composite jacket. Upon completion of the curing period, all specimens were directly subjected to tensile testing without any additional post-curing or surface treatment.

3- Experimental Design

To investigate the mechanical behavior of the strengthened specimens under stepwise tensile loading, a series of tensile tests were conducted using an STM-250 universal testing machine. Unlike conventional monotonic tensile testing, in which the load is applied continuously until failure, the loading protocol adopted in this study consisted of multiple discrete loading stages separated by prescribed holding periods under constant displacement. This approach enabled the mechanical response of the strengthened specimens to be evaluated under conditions more representative of practical service environments, where structural components are frequently subjected to intermittent loading rather than continuous monotonic loading.

Consequently, in addition to evaluating the load-carrying capacity of the strengthened joint, the proposed loading protocol also allowed the investigation of time-dependent phenomena, including stress redistribution, displacement evolution during the holding periods, and the viscoelastic response of the epoxy matrix within the reinforced region. Figure 1 illustrates a GFRP-strengthened specimen during the tensile test. Prior to the main experimental program, a preliminary tensile test was performed at a loading rate of 10 mm/min. This test was conducted to verify the proper operation of the testing machine, ensure correct specimen alignment and gripping, and obtain a preliminary assessment of the mechanical response of the strengthened specimens under tensile loading. After confirming the reliability of the experimental setup, the main test program was carried out at loading rates of 50, 100, 150, and 200 mm/min. In all experiments, once the prescribed displacement for each loading stage was reached, the crosshead displacement was held constant for 10 min before the subsequent loading stage commenced. These holding periods were introduced to evaluate the time-dependent response of the strengthened system and to monitor the evolution of stress and displacement during the interruption of loading.

At the loading rate of 50 mm/min, the loading history consisted of three consecutive stages, each corresponding to a displacement increment of 1 mm. The specimen was first loaded to a displacement of 1 mm, followed by a 10 min holding period. The loading was then resumed to 2 mm, followed by another holding period, and subsequently repeated until a cumulative displacement of 3 mm was reached. After completion of the final holding period, the specimen was loaded continuously until failure. For the higher loading rates of 100, 150, and 200 mm/min, the loading sequence was divided into four stages to provide more gradual loading and improved control of the loading process. In these tests, each stage corresponded to a displacement increment of 0.75 mm, resulting in the same cumulative displacement of 3 mm after the fourth stage. Similar to the previous loading protocol, each loading stage was followed by a 10 min holding period under constant displacement before the next stage was initiated. Upon completion of the fourth holding period, continuous tensile loading was resumed until specimen failure. The experimental program was designed such that the cumulative displacement applied during the staged loading sequence remained constant at 3 mm for all loading rates, while only the loading rate and the loading sequence were varied. This approach enabled a direct evaluation of the influence of loading rate, stepwise loading history, and intermediate holding periods on the mechanical behavior of the strengthened region, thereby providing a consistent basis for comparing the response of the specimens under different loading conditions. The details of the experimental program are summarized in Table 1. To quantify the mechanical response of the strengthened joint, the shear stress was calculated based on the applied tensile load and the effective shear area of the strengthened region. The effective shear area was determined by considering the circumference of the reinforced section and the effective shear length. Accordingly, the effective shear area was calculated using Equation (1):

$$A = 2\pi\left(\frac{D}{2} + t\right)L \tag{1}$$

where (D) is the outer diameter of the steel pipe, (t) is the wall thickness of the steel pipe, and (L) is the effective shear length of the strengthened region. For the specimens investigated in this study, (D=25.4) mm, (t=3.38) mm, and (L=75) mm were considered. The shear stress was then calculated using Equation (2):

$$\tau = \frac{P}{A} \tag{2}$$

where (P) is the applied tensile load and (τ) is the shear stress in the strengthened region. The calculated shear stress values were subsequently used to evaluate the stress evolution during the successive loading stages and to determine the ultimate shear stress at failure. Considering the time-consuming fabrication process of the strengthened specimens, the sensitivity of the surface preparation and composite curing procedures, the limited availability of laboratory testing facilities, and the relatively high cost associated with specimen fabrication and mechanical testing, only one specimen was tested for each experimental condition. Therefore, the results presented in this study are intended to identify the overall trends in the mechanical behavior under different loading conditions. Repeated experiments with statistical analysis are recommended as a subject for future research to further validate the observed trends.

Table 1 Experimental Design

Row	Loading Rate (mm/min)	Test Type	Loading Type	Holding Time at Each Loading Step (min)
1	10	Pre-Test	Monotonic Tensile Test	-
2	50	Main Test	Step 1 Tensile Loading	**10**
3	50	Main Test	Step 2 Tensile Loading	**10**
4	50	Main Test	Step 3 Tensile Loading	**10**
5	100	Main Test	Step 1 Tensile Loading	**10**
6	100	Main Test	Step 2 Tensile Loading	**10**
7	100	Main Test	Step 3 Tensile Loading	**10**
8	100	Main Test	Step 4 Tensile Loading	**10**
9	150	Main Test	Step 1 Tensile Loading	**10**
10	150	Main Test	Step 2 Tensile Loading	**10**
11	150	Main Test	Step 3 Tensile Loading	**10**
12	150	Main Test	Step 4 Tensile Loading	**10**
13	200	Main Test	Step 1 Tensile Loading	**10**
14	200	Main Test	Step 2 Tensile Loading	**10**
15	200	Main Test	Step 3 Tensile Loading	**10**
16	200	Main Test	Step 4 Tensile Loading	**10**



Fig. 1 GFRP-strengthened specimen mounted in the tensile testing machine

4- Results and Discussion

This section presents and discusses the mechanical response of the GFRP-strengthened steel pipe specimens subjected to stepwise tensile loading. The primary objective is to evaluate the response of the strengthened system to the stepwise loading protocol and to investigate the influence of intermediate holding periods on stress evolution and the overall mechanical behavior. Furthermore, the effects of different loading rates on the initial stiffness, joint stability, and failure characteristics are examined and compared. The overall experimental results are summarized in Table 2. The experimental data and corresponding stress–displacement curves provide a comprehensive basis for evaluating the mechanical performance of the strengthened region and the effectiveness of the GFRP composite reinforcement. A detailed analysis and interpretation of each result are presented in the following sections.

Table 2. Summary of the Experimental Results

Row	Loading Rate (mm/min)	Test Type	Loading Type	Holding Time at Each Loading Step (min)	Shear Stress at the End of Each Loading Step (MPa)	Shear Stress After Stress Relaxation at the End of Each Loading Step (MPa)	Stress Relaxation Percentage at Each Loading Step (%)	Ultimate Shear Stress (MPa)
1	10	Pre-Test	Monotonic Tensile Test	-	-	-	-	5.886
2	50	Main Test	Step 1 Tensile Loading	10	1.605	1.54	6.5	5.485
3	50	Main Test	Step 2 Tensile Loading	10	3.228	3.051	17.7	
4	50	Main Test	Step 3 Tensile Loading	10	4.552	4.143	40.9	
5	100	Main Test	Step 1 Tensile Loading	10	0.729	0.680	4.9	4.463
6	100	Main Test	Step 2 Tensile Loading	10	1.822	1.712	11	
7	100	Main Test	Step 3 Tensile Loading	10	2.711	2.536	17.5	
8	100	Main Test	Step 4 Tensile Loading	10	3.465	3.136	32.9	
9	150	Main Test	Step 1 Tensile Loading	10	0.543	0.514	2.9	4.724
10	150	Main Test	Step 2 Tensile Loading	10	1.257	1.186	7.1	
11	150	Main Test	Step 3 Tensile Loading	10	2.005	1.878	12.7	
12	150	Main Test	Step 4 Tensile Loading	10	2.666	2.487	17.9	
13	200	Main Test	Step 1 Tensile Loading	10	0.287	0.268	1.9	4.424
14	200	Main Test	Step 2 Tensile Loading	10	0.978	0.919	5.9	
15	200	Main Test	Step 3 Tensile Loading	10	1.836	1.712	12.4	
16	200	Main Test	Step 4 Tensile Loading	10	2.541	2.343	19.8	

4-1-Preliminary Test

Figure 2 presents the tensile response of the strengthened specimen obtained from the preliminary test conducted at a loading rate of 10 mm/min. This preliminary test was performed to verify the proper operation of the testing system, ensure correct specimen alignment within the grips, evaluate the overall behavior of the strengthened joint prior to the main experimental program, and estimate the approximate load-carrying capacity of the system. Based on the results of this test, the target displacement levels, the number of loading stages, and the loading protocol adopted in the subsequent stepwise tensile tests were determined to prevent premature failure or the application of inappropriate loading levels. Since the purpose of this stage was limited to calibration and experimental design, the specimen was loaded continuously to failure without introducing intermediate holding periods. Consequently, the obtained results were used solely as a reference for defining the loading parameters of the main experimental program. At the beginning of the test, the stress increased gradually, primarily due to specimen seating within the testing grips and the elimination of initial clearances. After this initial region, the stress–displacement curve exhibited a nearly linear and stable response, indicating efficient stress transfer through the epoxy adhesive and the GFRP reinforcement, as well as predominantly elastic behavior of the strengthened system before the onset of damage. As the displacement approached approximately 5 mm, the slope of the curve gradually decreased, suggesting the initiation of internal damage mechanisms within the strengthened joint. This behavior can be attributed to the formation of microcracks within the epoxy matrix, the initiation of local interfacial debonding, or the accumulation of microscopic damage in the composite layer. The maximum shear stress recorded during the test was 5.886 MPa, corresponding to the onset of the final failure process. Immediately after reaching the peak stress, a sudden and pronounced stress drop occurred, indicating brittle failure of the primary load-transfer mechanism. The abrupt reduction in load-carrying capacity suggests that failure propagated rapidly through the bonded region without significant damage evolution or plastic deformation. Nevertheless, the stress did not decrease directly to zero. Instead, a small secondary peak accompanied by a residual stress plateau was observed, indicating that, following the primary failure, a limited amount of load continued to be transferred through secondary mechanisms such as frictional resistance, mechanical interlocking of the remaining glass fibers, and localized adhesion between the composite jacket and the steel substrate. This post-failure response demonstrates that, although the bonded joint lost its primary structural integrity, these secondary load-transfer mechanisms temporarily resisted complete slippage and delayed the total loss of load-carrying capacity.

4-2- Stepwise Loading at a Loading Rate of 50 mm/min

Figure 3 illustrates the mechanical response of the strengthened specimen subjected to stepwise tensile loading at a loading rate of 50 mm/min. In this test, loading was applied in three successive stages, with the specimen held at a constant displacement for 10 min after each stage before loading resumed continuously until final failure. This loading protocol enabled the evaluation of the mechanical response of the strengthened joint under gradual loading conditions and provided insight into the time-dependent behavior of the system during the holding periods. During the first loading stage (Step 1), the shear stress increased almost linearly with displacement, indicating predominantly elastic behavior of the strengthened joint.

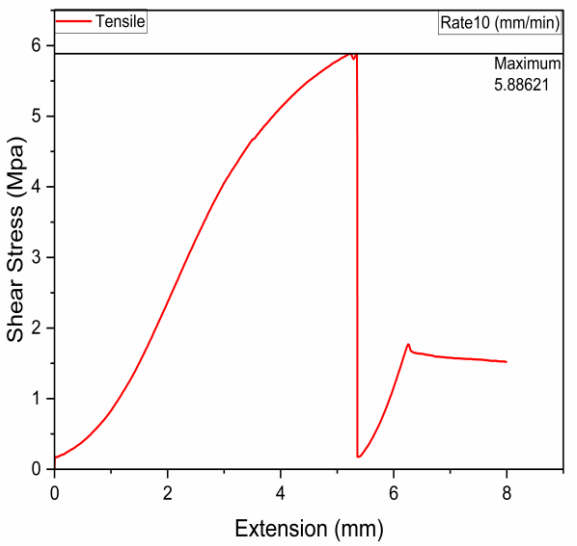


Fig 2. Preliminary tensile test conducted at a loading rate of 10 mm/min

Upon reaching the prescribed displacement, loading was interrupted, and the specimen was maintained under constant displacement for 10 min. During this holding period, the stress–displacement curve exhibited an approximately horizontal trend, reflecting the time-dependent response of the joint under constant displacement. This behavior can be attributed to stress redistribution within the bonded region and the viscoelastic relaxation of the epoxy matrix. When the second loading stage (Step 2) commenced, the shear stress increased again and reached approximately 3.2 MPa before the second holding period was introduced. Similar to the previous stage, the stress remained nearly constant during the 10-min interruption, indicating the continuation of time-dependent stress evolution within the strengthened system. The same trend was observed during the third loading stage (Step 3), where the shear stress increased to approximately 4.5 MPa before the final holding period. After completion of the three loading stages and attainment of a cumulative displacement of 3 mm, continuous tensile loading was resumed until specimen failure. The specimen reached a maximum shear stress of 5.485 MPa, after which a sudden and significant stress drop occurred, indicating brittle failure of the strengthened joint. Despite the substantial loss of load-carrying capacity, the stress did not immediately decrease to zero. Instead, a small secondary peak together with a residual stress level was observed after the primary failure. This post-failure behavior suggests that a limited amount of load continued to be transferred through secondary mechanisms, including friction between the fractured surfaces, localized mechanical interlocking of the remaining glass fibers, and residual adhesion within the bonded region.

4-3- Stepwise Loading at a Loading Rate of 100 mm/min

Figure 4 illustrates the mechanical response of the strengthened specimen subjected to stepwise tensile loading at a loading rate of 100 mm/min. In this test, loading was applied in four stages, each corresponding to a displacement increment of 0.75 mm.

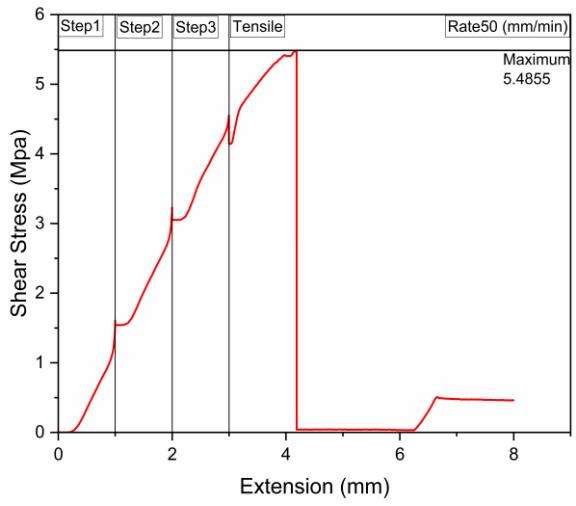


Fig 3. Stepwise tensile loading at a loading rate of 50 mm/min

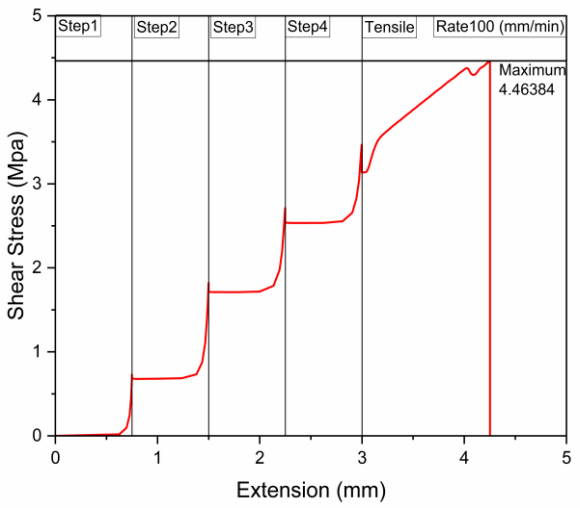


Fig 4. Stepwise tensile loading at a loading rate of 100 mm/min

After each loading stage, the specimen was held at a constant displacement for 10 min before the subsequent stage commenced. This loading protocol enabled the mechanical response of the strengthened joint to be evaluated throughout the loading sequence and allowed the influence of the holding periods on the time-dependent behavior of the system to be assessed. During the first loading stage (Step 1), the shear stress increased almost linearly with displacement. Once the prescribed displacement was reached, loading was interrupted, and the stress–displacement curve entered an approximately horizontal region during the 10-min holding period, indicating the time-dependent response of the strengthened joint under constant displacement. At the beginning of the second loading stage (Step 2), the shear stress increased again and reached approximately 1.8 MPa, after which the specimen was maintained under constant displacement for another 10 min. Similar behavior to that observed during the first stage was recorded, reflecting continued stress redistribution and viscoelastic relaxation within the composite-strengthened joint. The same trend was observed during the third (Step 3) and fourth (Step 4) loading stages, where the shear stress continued to increase progressively, demonstrating the ability of the bonded joint to sustain additional load throughout the staged loading sequence. After completion of the fourth loading stage and attainment of a cumulative displacement of 3 mm, continuous tensile loading was resumed until failure. The specimen reached a maximum shear stress of 4.463 MPa, followed by a sudden stress drop, indicating brittle failure of the strengthened joint. Overall, the results demonstrate that, at a loading rate of 100 mm/min, the strengthened joint was capable of sustaining progressively increasing stress throughout the stepwise loading sequence. Nevertheless, the final failure remained abrupt and brittle, indicating that the staged loading history altered the stress evolution but did not change the fundamental failure mechanism of the GFRP-strengthened joint.

4-4- Stepwise Loading at a Loading Rate of 150 mm/min

Figure 5 presents the mechanical response of the strengthened specimen subjected to stepwise tensile loading at a loading rate of 150 mm/min. Similar to the 100 mm/min loading protocol, the test consisted of four loading stages, each corresponding to a displacement increment of 0.75 mm. After each loading stage, the specimen was maintained at a constant displacement for 10 min, after which the subsequent loading stage was initiated.

During the first loading stage (Step 1), the shear stress increased steadily with displacement, followed by an approximately horizontal region during the holding period, indicating the time-dependent response of the strengthened joint under constant displacement. A similar trend was observed throughout the second, third, and fourth loading stages, with the shear stress increasing progressively to approximately 1.2 MPa, 2.0 MPa, and 2.6 MPa, respectively. At the end of each loading stage, the stress remained nearly constant throughout the 10-min holding period, reflecting the continued time-dependent response associated with stress redistribution and the viscoelastic behavior of the epoxy matrix.

Following completion of the four loading stages and attainment of a cumulative displacement of 3 mm, continuous tensile loading was resumed until failure. The specimen reached a maximum shear stress of 4.724 MPa, after which a sudden and pronounced stress drop occurred, indicating brittle failure of the strengthened joint. A small residual stress remained after the primary failure, suggesting that a limited amount of load continued to be transferred through secondary mechanisms, including friction between the fractured surfaces, localized mechanical interlocking of the remaining glass fibers, and residual adhesion within the bonded region. An interesting observation is that, despite the overall reduction in load-carrying capacity with increasing loading rate, the maximum shear stress measured at 150 mm/min was slightly higher than that obtained at 100 mm/min. Since only one specimen was tested for each loading condition, this difference cannot be conclusively attributed to a specific physical mechanism. Instead, it may reflect the inherent scatter of experimental results, minor variations in specimen fabrication, local differences in bond quality, or unavoidable uncertainties associated with the testing procedure. Nevertheless, the maximum shear stress recorded at 150 mm/min remained lower than that obtained at 50 mm/min, and the overall experimental results consistently indicate that increasing the loading rate leads to a reduction in the load-carrying capacity of the strengthened joint.

4-5- Stepwise Loading at a Loading Rate of 200 mm/min

Figure 6 presents the mechanical response of the strengthened specimen subjected to stepwise tensile loading at a loading rate of 200 mm/min. Similar to the tests conducted at 100 and 150 mm/min, the loading sequence consisted of four consecutive stages, each corresponding to a displacement increment of 0.75 mm.

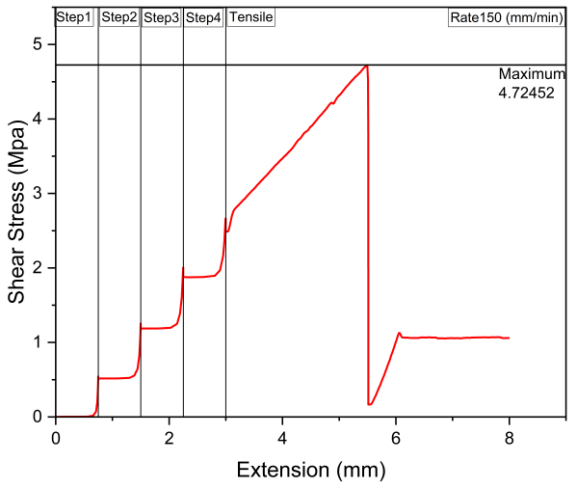


Fig 5. Stepwise tensile loading at a loading rate of 150 mm/min

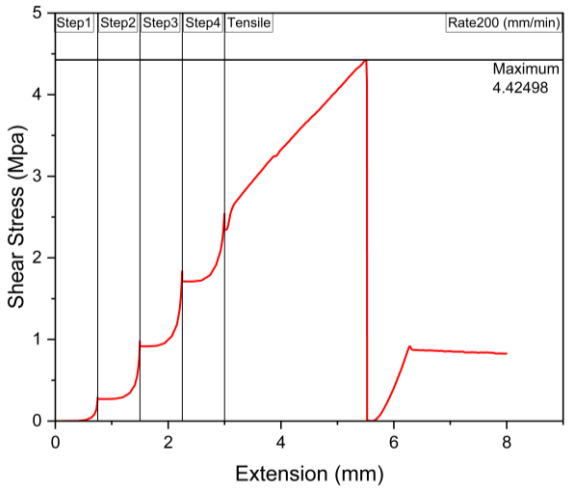


Fig 6. Stepwise tensile loading at a loading rate of 200 mm/min

After each loading stage, the specimen was maintained at a constant displacement for 10 min, after which the subsequent loading stage was initiated. During the first loading stage (Step 1), the shear stress increased more rapidly than that observed at the lower loading rates. Once the prescribed displacement was reached, loading was interrupted, and the stress–displacement curve entered an approximately horizontal region, representing the time-dependent response of the strengthened joint during the holding period. Similar behavior was observed throughout the second, third, and fourth loading stages, with the shear stress increasing progressively to approximately 1.0 MPa, 1.8 MPa, and 2.5 MPa, respectively. At this loading rate, the stress variations during the holding periods were less pronounced than those observed at the lower loading rates, and the stress–displacement curve transitioned more rapidly to the subsequent loading stage. After completion of the four loading stages and attainment of a cumulative displacement of 3 mm, continuous tensile loading was resumed until failure. The specimen reached a maximum shear stress of 4.424 MPa, after which a sudden stress drop occurred, indicating brittle failure of the strengthened joint. A small residual stress remained after the primary failure, suggesting that a limited amount of load continued to be transferred through secondary mechanisms such as friction between the fractured surfaces, localized mechanical interlocking of the remaining fibers, and residual adhesion within the bonded region.

Overall, the results demonstrate that increasing the loading rate to 200 mm/min resulted in a reduction in the ultimate load-carrying capacity compared with the specimen tested at 150 mm/min. Furthermore, the less pronounced stress variations observed during the holding periods indicate that the contribution of time-dependent mechanisms, including viscoelastic relaxation and stress redistribution within the bonded joint, becomes less significant as the loading rate increases.

4-6- Overall Tensile Response under Stepwise Loading at Different Loading Rates

Figure 7 compares the tensile responses of the strengthened specimens tested at loading rates of 50, 100, 150, and 200 mm/min, providing a direct assessment of the influence of loading rate on the mechanical behavior of the strengthened joint. Although all specimens exhibited a similar overall trend, characterized by a progressive increase in shear stress followed by abrupt brittle failure, noticeable differences were observed in the initiation of each loading stage and in the overall shape of the stress–displacement curves.

.

At the loading rate of 50 mm/min, the stress increased almost immediately upon the initiation of each loading stage, with little or no horizontal region preceding the stress increase. In contrast, at loading rates of 100, 150, and 200 mm/min, a short region with a very small slope or an approximately horizontal response appeared at the beginning of each loading stage. During this region, the displacement increased while the corresponding increase in shear stress remained limited. This observation indicates that the initial mechanical response following each holding period differs between the lower and higher loading rates. The presence of these nearly horizontal regions at higher loading rates suggests that part of the initial displacement after each holding period was consumed in re-establishing effective load transfer across the bonded interface before a significant increase in stress occurred. By comparison, this phenomenon was negligible or absent at the loading rate of 50 mm/min, where stress transfer resumed almost immediately after loading recommenced. Nevertheless, the exact mechanisms responsible for this behavior cannot be conclusively identified based solely on the present experimental results. Additional investigations, including microstructural characterization and further time-dependent experimental studies, are required to clarify the underlying mechanisms. Overall, Figure 7 demonstrates that increasing the loading rate influences not only the ultimate load-carrying capacity of the strengthened joint but also the mechanical response at the beginning of each loading stage, resulting in a modified initial response following each intermediate holding period.

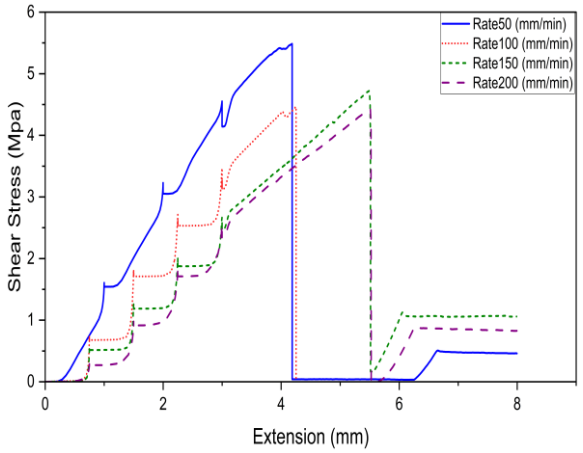


Fig 7. Stepwise tensile stress–displacement curves at different loading rates

4-7- Bar charts of the stepwise tensile response at different loading rates

Figure 8 presents the shear stress measured at the end of each loading stage for the four loading rates of 50, 100, 150, and 200 mm/min. The results indicate that, in general, increasing the loading rate led to a reduction in the shear stress attained at the end of each loading stage, although the magnitude of this reduction varied from one stage to another. During Stage 1, the shear stress decreased from 1.605 MPa at 50 mm/min to 0.729, 0.543, and 0.287 MPa at loading rates of 100, 150, and 200 mm/min, respectively, corresponding to reductions of approximately 55%, 66%, and 82% relative to the 50 mm/min condition. These results demonstrate that the first loading stage exhibited the greatest sensitivity to increases in loading rate.

A similar trend was observed during Stage 2, where the shear stress decreased from 3.228 MPa at 50 mm/min to 1.822, 1.257, and 0.978 MPa at loading rates of 100, 150, and 200 mm/min, respectively, representing reductions of approximately 43%, 61%, and 70%, respectively. During Stage 3, the shear stress decreased from 4.552 MPa at 50 mm/min to 2.711, 2.005, and 1.836 MPa at 100, 150, and 200 mm/min, respectively, corresponding to reductions of approximately 40%, 56%, and 60%, respectively. Compared with the previous stages, the magnitude of the reduction became less pronounced, indicating that the influence of loading rate gradually diminished as loading progressed. Stage 4 was performed only for the specimens tested at 100, 150, and 200 mm/min. The measured shear stress decreased from 3.465 MPa at 100 mm/min to 2.666 MPa and 2.541 MPa at 150 and 200 mm/min, respectively, corresponding to reductions of approximately 24% and 27%. These results indicate that the differences among the higher loading rates became considerably smaller during the final loading stage. Overall, Figure 8 demonstrates that the influence of loading rate was most significant during the early stages of stepwise loading. As the number of loading stages increased, the differences in shear stress among the various loading rates gradually decreased, suggesting that the sensitivity of the strengthened joint to loading rate diminished with progressive loading.

4-8- Bar charts of stress relaxation at each loading stage

Figure 9 presents the reduction in shear stress during the 10-min holding periods at different loading stages and loading rates. The values shown in this figure were calculated as the difference between the shear stress recorded immediately before the loading interruption and the stress measured after the 10-min constant-displacement holding period.

Therefore, the results quantify the stress reduction that occurred during each holding period and enable a direct comparison of the time-dependent response under different loading rates. During Stage 1, the stress reduction decreased from 0.065 MPa at 50 mm/min to 0.049, 0.029, and 0.019 MPa at loading rates of 100, 150, and 200 mm/min, respectively. These values correspond to reductions of approximately 24%, 55%, and 70% relative to the specimen tested at 50 mm/min. A similar trend was observed during Stage 2, where the stress reduction decreased from 0.177 MPa at 50 mm/min to 0.110, 0.071, and 0.059 MPa at loading rates of 100, 150, and 200 mm/min, respectively. During Stage 3, the largest stress reduction was again recorded for the specimen tested at 50 mm/min, reaching 0.409 MPa. Compared with this value, the stress reduction at loading rates of 100, 150, and 200 mm/min was approximately 57%, 69%, and 70% lower, respectively. Stage 4 was performed only for the specimens tested at 100, 150, and 200 mm/min. In this stage, the stress reduction decreased from 0.329 MPa at 100 mm/min to 0.179 MPa and 0.198 MPa at loading rates of 150 and 200 mm/min, respectively. Overall, Figure 9 demonstrates that, within the 10-min holding period, specimens tested at lower loading rates experienced greater stress reduction than those tested at higher loading rates. This observation indicates that the time-dependent response of the GFRP-strengthened joint is influenced by

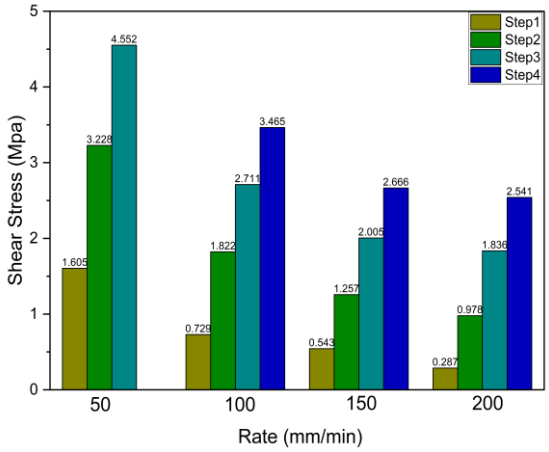


Fig 8. Shear stress at the end of each loading stage under different loading rates

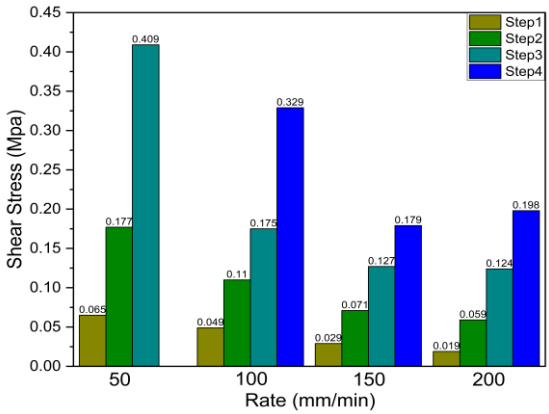


Fig 9. Shear stress reduction during each loading stage

the loading rate, with higher loading rates resulting in less pronounced stress reduction during the holding periods.

4-9- Bar charts of the stepwise tensile response at different loading rates

Figure 10 compares the maximum shear stress recorded during the stepwise tensile tests at loading rates of 50, 100, 150, and 200 mm/min. The results indicate that the highest shear stress, 5.485 MPa, was obtained at the loading rate of 50 mm/min. Increasing the loading rate to 100 mm/min reduced the maximum shear stress to 4.463 MPa, corresponding to a decrease of approximately 19% relative to the specimen tested at 50 mm/min. This reduction indicates that increasing the loading rate under stepwise loading conditions adversely affects the ultimate load-carrying capacity of the strengthened joint. At a loading rate of 150 mm/min, the maximum shear stress increased slightly to 4.724 MPa compared with the value obtained at 100 mm/min, although it remained lower than that recorded at 50 mm/min. Since only one specimen was tested under each loading condition, this modest increase cannot be conclusively attributed to a specific physical mechanism. Instead, it is likely to fall within the inherent experimental scatter and may result from minor variations in specimen fabrication, bond quality, or testing conditions. When the loading rate was further increased to 200 mm/min, the maximum shear stress decreased again to 4.424 MPa, representing the lowest value among all stepwise loading tests. Overall, although the variation in maximum shear stress was not perfectly monotonic, increasing the loading rate from 50 to 200 mm/min resulted in an overall reduction of approximately 19% in the ultimate load-carrying capacity of the strengthened joint. Furthermore, the relatively small

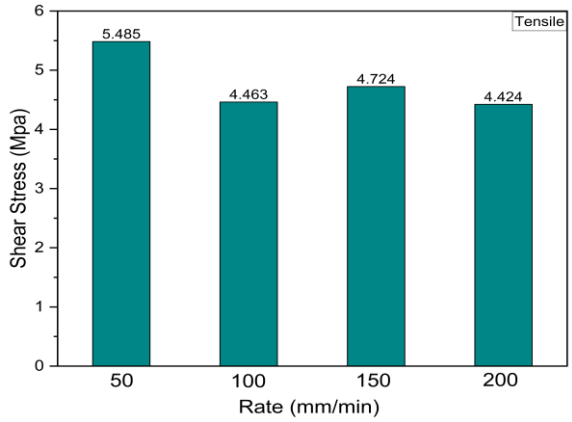


Fig 10. Bar chart of the ultimate tensile strength at different loading rates

difference between the results obtained at 100 and 150 mm/min should not be interpreted as evidence of a distinct change in the mechanical behavior of the system. Rather, it suggests that the mechanical response is influenced not only by the loading rate but also by unavoidable experimental factors, including minor variations in specimen fabrication, composite lay-up uniformity, adhesive bond quality, and the inherent scatter of experimental measurements. Moreover, when these results are considered together with the shear stress measured at the end of each loading stage (Figure 8) and the stress reduction during the holding periods (Figure 9), a consistent trend becomes evident. Specimens tested at lower loading rates not only sustained higher shear stresses throughout the individual loading stages but also exhibited higher ultimate shear stresses at failure. This agreement among the different experimental observations indicates that, under the present testing conditions, the dominant effect of increasing the loading rate was a gradual reduction in the ultimate load-carrying capacity of the GFRP-strengthened joint.

5- Conclusions

This study experimentally investigated the mechanical behavior of GFRP-strengthened steel pipes subjected to stepwise tensile loading with intermediate holding periods at different loading rates. The primary objective was to evaluate the effects of loading rate and loading history on the ultimate load-carrying capacity, shear stress evolution during successive loading stages, and stress reduction during the holding periods. The results demonstrated that the mechanical response of the strengthened joint is governed not only by the applied load level but also by the loading rate and loading history. The stepwise tensile tests showed that all specimens exhibited relatively stable and controlled mechanical responses before reaching their ultimate capacity, followed by sudden final failure. In general, an increase in the loading rate resulted in a reduction in the ultimate load-carrying capacity. However, a slight increase in the ultimate shear stress was observed at a loading rate of 150 mm/min compared with that at 100 mm/min. This limited variation can reasonably be considered to fall within the range of natural experimental scatter and minor unavoidable variations in specimen fabrication and testing conditions. Overall, the dominant trend of the results indicates a reduction in ultimate capacity with increasing loading rate.

Comparison of the shear stress at different loading stages showed that the effect of loading rate was more pronounced during the early stages of loading and became less significant as loading progressed. During Stage 1, the shear stress at the end of the loading stage decreased noticeably as the loading rate increased from 50 to 100, 150, and 200 mm/min. A similar trend was observed during Stages 2 and 3, although the magnitude of the differences gradually decreased in the subsequent stages. These findings indicate that the loading rate affects not only the ultimate capacity of the strengthened joint but also the evolution of shear stress throughout the loading history.

Analysis of stress evolution during the 10-min holding periods showed that the magnitude of stress reduction was greater at lower loading rates. This behavior indicates that the time-dependent response of the strengthened joint is influenced by the loading rate. The viscoelastic behavior of the epoxy resin, together with the gradual redistribution of stress between the GFRP layers and the steel pipe, may contribute to this behavior. However, since the holding period was limited to 10 min, a definitive separation of the contribution of viscoelastic relaxation from other possible mechanisms, such as localized interfacial slip or bond degradation, requires further investigation.

Comparison of the different loading stages demonstrated that increasing the loading rate can affect stress transfer and redistribution throughout the loading history, with this effect being more pronounced during the early loading stages. In addition, the intermediate holding periods resulted in a gradual reduction in stress and a change in the mechanical state of the specimen before the subsequent loading stage. Therefore, the loading rate, the number and sequence of loading stages, and the holding duration should be considered simultaneously when evaluating the performance of GFRP-strengthened steel joints.

From an engineering perspective, the results indicate that using the ultimate capacity obtained from conventional continuous loading as the sole criterion for evaluating strengthened joints subjected to staged and variable loading may not fully represent their actual mechanical behavior. Given the limited number of specimens and the specific experimental conditions considered in this study, determining a specific safety factor based solely on the present results is not recommended. Nevertheless, the observed reduction in capacity at higher loading rates highlights the importance of considering loading-rate and loading-history effects in the assessment and design of GFRP-strengthened joints.

Further studies are recommended to systematically investigate the effects of temperature, holding duration between loading stages, number of loading stages, and load magnitude at each stage. In addition, repeated tests under each loading condition and a detailed investigation of the failure mechanisms and steel–GFRP interface behavior would provide a better assessment of experimental variability, improve the generalizability of the findings, and contribute to a more comprehensive understanding of the mechanisms governing the time-dependent response of the strengthened system.

Overall, the findings of this study demonstrate that the behavior of GFRP-strengthened steel pipes under stepwise loading results from the combined effects of loading rate, loading history, and the time-dependent response of the composite strengthening system. These results provide a basis for further investigations and the development of more reliable approaches for the assessment and design of GFRP-strengthened structures and pipelines subjected to realistic and variable loading conditions.

Ethics Approval: The scientific content of this article is the result of the authors' research and has not been published in any other journal.

Conflict of Interest: There are no conflicts of interest to declare.

Artificial Intelligence Statement: The authors used ChatGPT for text revision, grammatical improvement, and translation of parts of the manuscript. The resulting text was carefully reviewed and edited, and the authors assume full responsibility for the accuracy, originality, and final content of the manuscript.

Funding: This research received no financial support from any funding agency, organization, or institution.

Author Contributions: The first author is responsible for preparing the initial draft of the manuscript, creating the figures and charts, and analyzing the results, with a 50% contribution to the study. The second author is responsible for supervising the research and conducting the final editing of the manuscript, with a 50% contribution to the study.

6- References

[1] M. Shamsuddoha, M. M. Islam, T. Aravinthan, A. Manalo, and K.-t. Lau, "Effectiveness of using fibre-reinforced polymer composites for underwater steel pipeline repairs," *Composite Structures,* vol. 100, pp. 40–54, 2013. doi: 10.1016/j.compstruct.2012.12.019

[2] F. Taheri, "Advanced fiber-reinforced polymer (FRP) composites for the manufacture and rehabilitation of pipes and tanks in the oil and gas industry," in *Advanced Fibre-Reinforced Polymer (FRP) Composites for Structural Applications*: Elsevier, 2013, pp. 662–704. doi: 10.1533/9780857098641.4.662

[3] K. Beklemysheva, A. Vasyukov, V. Golubev, and Y. I. Zhuravlev, "On the estimation of seismic resistance of modern composite oil pipeline elements," in *Doklady Mathematics*, 2018, vol. 97, no. 2: Springer, pp. 184–187. doi: 10.1134/S1064562418020011

[4] L. T. Popoola, A. S. Grema, G. K. Latinwo, B. Gutti, and A. S. Balogun, "Corrosion problems during oil and gas production and its mitigation," *International Journal of Industrial Chemistry,* vol. 4, no. 1, p. 35, 2013. doi: 10.1186/2228-5547-4-35

[5] P. Laney, "Use of composite pipe materials in the transportation of natural gas," *INEEL Field Work Proposal,* vol. 70, p. 4340, 2002.

[6] G. O. Edah, J. O. Atiba, and O. S. Fayomi, "Advancements in fibre-reinforced polymers: Properties, applications (A mini review)," *Next Materials,* vol. 8, p. 100743, 2025. doi: 10.1016/j.nxmate.2025.100743

[7] K. S. Lim, S. Azraai, N. Noor, and N. Yahaya, "An overview of corroded pipe repair techniques using composite materials," *Int. J. Mater. Metall. Eng,* vol. 10, no. 1, pp. 19–25, 2016.

[8] E. Alrehaili, A. Nurdiawati, and S. G. Al-Ghamdi, "Sustainable composites for metal replacement: Environmental assessment and material selection of fiber-reinforced polymer across industries," *Resources, Conservation & Recycling Advances,* p. 200294, 2025. doi: 10.1016/j.rcradv.2025.200294

[9] F. G. Alabtah and E. Mahdi, "The effect of sizing optimization on the interface between high strength steel and fiber reinforced composite," *Composite Structures,* vol. 266, p. 113740, 2021. doi: 10.1016/j.compstruct.2021.113740

[10] "Sarkhosh R, Farrokhabadi A, Zarei H R. Experimental Investigation of Energy Absorption of Aluminum/ Composite Hybrid Tube Produced by Tape Winding Method under QuasiStatic Load. Modares Mechanical Engineering. 2021; 21(1):55-67.." doi: 20.1001.1.10275940.1399.21.1.6.0

[11] R. Beyranvand and m. ansari, "Experimental Investigation of the Effect of Tensile Pre Damage and Cyclic Loading on the Flexural Capacity of GFRP Strengthened Steel Pipes under Dry and Wet Environmental Conditions," *Modares Mechanical Engineering,* pp. –, 2026, doi: 10.48311/mme.2026.119730.82991.

[12] H. Wang, Q. Zong, and H. Wang, "Research on the tensile mechanical properties and fracture characteristics of GFRP mortar tubes under impact loads," *KSCE Journal of Civil Engineering,* vol. 28, no. 4, pp. 1367–1378, 2024. doi: 10.1007/s12205-024-0647-x

[13] J. S. Yuan *et al.*, "Flexural behaviour of concrete-filled pultruded GFRP box beams after exposure to elevated temperatures," *Engineering Structures,* vol. 357, p. 122497, 2026. doi: 10.1016/j.engstruct.2026.122497

[14] T. D'Antino and M. A. Pisani, "Use of bending test to determine the tensile strength and elastic modulus of GFRP bars," *Composite Structures,* vol. 323, p. 117424, 2023. doi: 10.1016/j.compstruct.2023.117424

[15] M. Noroozolyaee, D. Mostofinejad, A. Saljoughian, and A. Zamanvaziri, "Behavior of square concrete column reinforced with GFRP bars under new reversed cyclic eccentric loading: Experimental and analytical study," *Case Studies in Construction Materials,* p. e05598, 2025. doi: https://doi.org/10.1016/j.cscm.2025.e05598

[16] S. Ahankari and A. Patil, "Sea water effect on mechanical performance of steel pipes rehabilitated with glass fiber reinforced epoxy composites," *Materials Today: Proceedings,* vol. 22, pp. 2490–2498, 2020. doi: 10.1016/j.matpr.2020.03.377

[17] E. A. Esleman and G. Önal, "Three-point bending fatigue behavior of basalt-carbon-glass/epoxy hybrid composites under saltwater environment," *Fatigue & Fracture of Engineering Materials & Structures,* vol. 46, no. 7, pp. 2496–2509, 2023. doi: 10.1111/ffe.14012

[18] H. H. Arifin *et al.*, "Stress distribution analysis of composite repair with Carbon Nanotubes reinforced putty for damaged steel pipeline," *International Journal of Pressure Vessels and Piping,* vol. 194, p. 104537, 2021. doi: 10.1016/j.ijpvp.2021.104537

[19] J. M. George, M. Kimiaei, M. Elchalakani, and S. Fawzia, "Experimental and numerical investigation of underwater composite repair with fibre reinforced polymers in corroded tubular offshore structural members under concentric and eccentric axial loads," *Engineering Structures,* vol. 227, p. 111402, 2021. doi: 10.1016/j.engstruct.2020.111402

[20] R. Verde, A. D'Amore, and L. Grassia, "A Numerical Model to Predict the Relaxation Phenomena in Thermoset Polymers and Their Effects on Residual Stress during Curing—Part I: A Theoretical Formulation and Numerical Evaluation of Relaxation Phenomena,"

Polymers, vol. 16, no. 10, p. 1433, 2024. doi: 10.3390/polym16101433

[21] ""R. Beyranvand and M. Ansari, "Time Dependent Analysis of the Behavior of GFRP-Strengthened Steel Tubes under Stepwise Loading and Stress Relaxation," Mechanic of Advanced and Smart Materials, vol. 5, no. 1, pp. 146–170, 2025. doi: 10.52547/masm.5.1.146.